

## Diagnostic experiments at a 3 MeV test stand at Rutherford Appleton Laboratory (United Kingdom)<sup>a)</sup>

C. Gabor,<sup>1,b)</sup> D. C. Faircloth,<sup>2</sup> D. A. Lee,<sup>3</sup> S. R. Lawrie,<sup>2</sup> A. P. Letchford,<sup>2</sup> and J. K. Pozimski<sup>2,3</sup>

<sup>1</sup>*ASTeC Intense Beams Group, Rutherford Appleton Laboratory, Oxfordshire OX11 0QX, United Kingdom*

<sup>2</sup>*Isis Pulsed Spallation Neutron Source, Rutherford Appleton Laboratory, Oxfordshire OX11 0QX, United Kingdom*

<sup>3</sup>*Department of Physics, Imperial College of Science and Technology, London SW7 2AZ, United Kingdom*

(Presented 24 September 2009; received 25 September 2009; accepted 15 December 2009; published online 24 February 2010)

A front end is currently under construction consisting of a H<sup>-</sup> Penning ion source (65 keV, 60 mA), low energy beam transport (LEBT), and radio frequency quadrupole (3 MeV output energy) with a medium energy beam transport suitable for high power proton applications. Diagnostics can be divided either in destructive techniques such as beam profile monitor, pepperpot, slit-slit emittance scanner (preferably used during commissioning) or nondestructive, permanently installed devices such as photodetachment-based techniques. Another way to determine beam distributions is a scintillator with charge-coupled device camera. First experiments have been performed to control the beam injection into the LEBT. The influence of beam parameters such as particle energy and space-charge compensation on the two-dimensional distribution and profiles will be presented.

© 2010 American Institute of Physics. [doi:10.1063/1.3290858]

### I. INTRODUCTION

#### A. The front end test stand (FETS) collaboration

In order to contribute to the development of high power proton accelerators in the megawatt range, to prepare the way for an Isis upgrade, and to contribute to the UK design effort on neutrino factories<sup>1</sup> a FETS is being constructed at the Rutherford Appleton Laboratory in the UK.<sup>2</sup> The aim of FETS is to demonstrate the production of a 50–60 mA, 2 ms, 50 pps chopped beam at 3 MeV with sufficient beam quality. An overview of the components is given in Ref. 3. At the moment only the ion source is operational, measurements are carried out to characterize the source and commission the photodetachment beam profile monitor. Investigations of the beam through the actual detector and general beam transportation experiments including energy variations to improve the injection into the low energy beam transport (LEBT) are performed. The paper summarizes these first measurements providing a (qualitative) discussion without laying claim to being comprehensive.

#### B. Diagnostics related to FETS

Some well-known diagnostics such as slit-slit scanner in  $x$  and  $y$ , toroidal H<sup>-</sup> current measurements, and a longitudinal movable pepperpot device are in use. The latter consists of a grid, scintillator, and a charge-coupled device camera

with multichannel plate outside the vacuum<sup>4</sup> and can be also used to detect the two-dimensional (2D) spatial distribution by dismantling the grid plate.

Negative ions also offers the chance of nondestructive beam diagnostics by using photodetachment where laser light with sufficient energy is used to overcome the binding energy of the additional electron, then diagnostics can be carried out either on detached electrons or produced neutrals.<sup>5</sup> For that purpose a particle detector has been constructed<sup>6</sup> and is integrated in the differential pumping vessel (see Fig. 1), the whole beamline is shown in Fig. 3. The particle detector has to accelerate the detached electrons from their very low birth energy from <1 eV to  $\approx 2$  keV by an applied voltage to the “jacket.” The Einzel lens effect can be neglected since focusing occurs typically in a range of 90%–110% of the beam energy depending of either deceleration or acceleration potential. Here the 2 kV potential is less than 6% of the typical beam energy of 35 keV. Also negligible is the droop of the longitudinal potential. The shown dipole magnet in Fig. 1 bends then the particles into a Faraday cup and the charge is detected with a sensitive analog-to-digital converter. For the work presented here, the acceleration sheet (Fig. 1) was used to vary the external potential in order to investigate the H<sup>-</sup> transport.

#### C. Theoretical background

For high current ion beams the self-field created by the particles plays a dominant role. A particle beam sees repulsive forces according to the charge state and beam current and widens. The charged particles also create a beam potential according to the space charge which can act as an attractive potential of compensation particles. Those are of oppo-

<sup>a)</sup> Contributed paper, published as part of the Proceedings of the 13th International Conference on Ion Sources, Gatlinburg, Tennessee, September 2009.

<sup>b)</sup> Electronic mail: christoph.gabor@stfc.ac.uk.

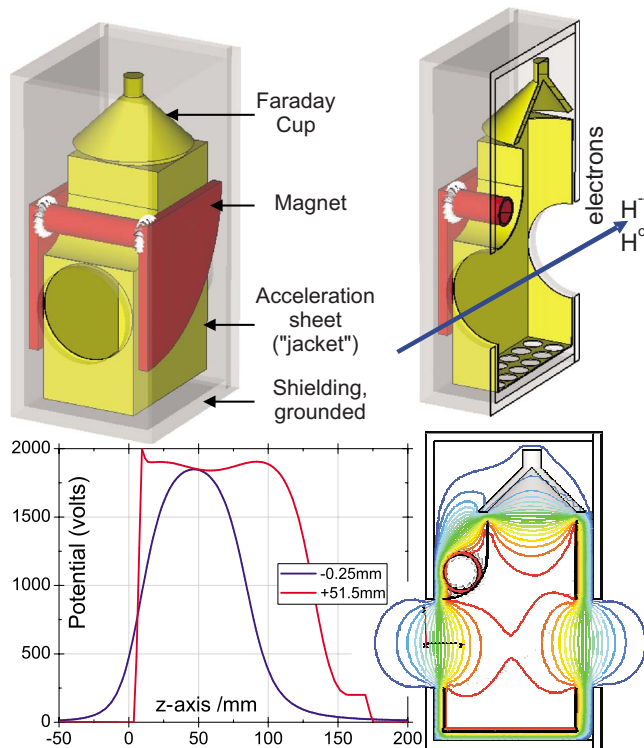


FIG. 1. (Color online) Overview of the detector arrangement to collect photodetached electrons.

site polarity of the beam ions and reduce the level of space-charge forces.<sup>7</sup> The space-charge compensation is also a dynamic process and typically needs several tens of  $\mu\text{s}$  to be established,<sup>8</sup> very often under circumstances such as gas pressure, interaction time, and external electromagnetic fields allow only a partial compensation. Measuring the current of the compensation particles depending of their energy can be used to determine the beam potential and hence, the level of compensation degree.

## II. EXPERIMENTAL SETUP AND ACHIEVED RESULTS

On the basis of the standard Isis Penning source the performance has been improved significantly in recent times.<sup>9</sup> A sketch of the ion source with its postacceleration system and the wiring of the power supplies is shown in Fig. 2. The beam is extracted through a  $(0.6 \times 10)$  mm slit in the aperture plate (plasma electrode) with a gap width of 2.3 mm gap between the extraction electrode and aperture plate. After extraction the beam is bent through a  $90^\circ$  sector magnet. The  $\text{H}^-$  beam emerges through a hole in the cold box and is further accelerated by a postextraction acceleration gap. Both the extraction voltage and the postacceleration determine the platform voltage, i.e., the total beam energy can be varied keeping constant the extraction. The further setup is shown in Fig. 3. This temporary setup was used to characterize the ion source and the beam at the entrance of the LEPT as well as carrying out experiments with the photodetachment profile monitor.

The maximum  $\text{H}^-$  current achieved so far was 69 mA in toroid 1 and 50 mA in toroid 2 which gives a transmission of 72% of transportable beam ready to inject into the solenoid

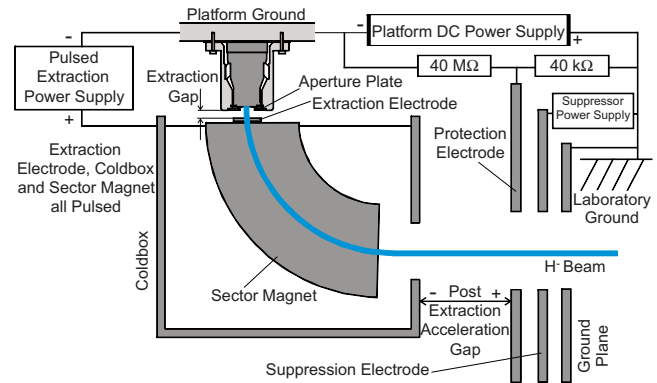


FIG. 2. (Color online) The schematic wiring of the FETS ion source and postacceleration system. The aperture plate of the Penning ion source has a slit extraction of  $0.6 \times 10$  mm, the separation of the jaws of the extraction electrode is 2.3 mm, and the spacing is 2.1 mm.

LEPT (at 18.8 kV extraction voltage and a platform voltage of 35 kV, i.e., a postacceleration of 16.2 kV). The position of the second toroid is where the first magnet of the LEPT will be placed.

To measure the beam profiles the scintillator is positioned as shown in Fig. 3. A voltage is applied to the jacket of the particle detector without laser operation. The detector is supplemented with an additional electrode in between the acceleration sheet and the Faraday cup to act as a secondary electron suppression. For the beam potential measurements the magnetic field was used to guide and maximize the compensation particles into the Faraday cup.

The typical gas pressure during ion source operation is two orders of magnitudes higher than without source operation. The pressure in the first section of the differential pumping tank is  $7.2 \times 10^{-5}$  mbar and in the diagnostics vessel is  $5.0 \times 10^{-5}$  mbar. If not otherwise stated, an extraction voltage of 12.5 kV is chosen and the beam energy for the space-charge investigations is 30 keV (the gap length of the postacceleration is set to 6 mm). For all pseudocolored 2D beam distributions shown the scale between pixel and millimeter is constant and is equivalent to 1 pixel  $\equiv 0.11024$  mm and the pictures span in  $x$  direction 980 and in  $y$  1125 pixels. The scintillator pictures are scaled according to their toroid measurements.

### A. Measurements with the postacceleration system

With the 2D distribution in Fig. 4 it is obvious that an increase postacceleration voltage has a positive effect of the beam transport. The increased beam energy of course reduces the space-charge forces but the pictures in Fig. 4 also imply a much stronger effect: The additional focusing and steering of equipotential lines curved outward producing a net force toward the beam axis. For extraction or postacceleration systems this effect is called electrode or aperture lens effect.<sup>10</sup> Thus, the higher the beam energy gets the more the beam shrinks and the current in toroid 2 increases whereas the current in toroid 1 increases only from 31 mA at 15 keV to 36.5 mA at  $\approx 18$  keV beam energy and then levels off, i.e., in general, the beam transport can be improved. The inner structure at 27.5 keV is very likely caused by the slit extrac-

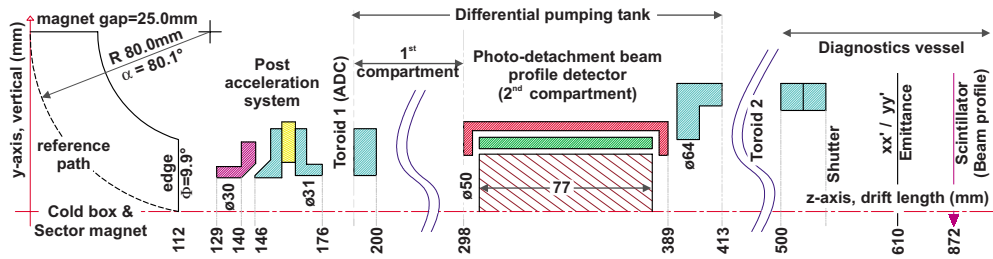


FIG. 3. (Color online) Current setup of FETS consisting of the ion source, differential pumping tank, and diagnostics vessel. The detector for the photodetachment beam profile monitor is integrated in the second chamber of the pumping tank. The scintillator for beam profiling is shown fully withdrawn; it can be moved up to the shutter. Pressure measurement gauges are installed at the ion source, in the first part of the differential stage, and in the diagnostics vessel.

tion and the transport through the dipole with a gradient. As the postacceleration gets higher the lens effect produces a focus (near 37 keV beam energy) and eventually overfocuses. This implies that for each current level and extraction level the correct postacceleration should be adopted. Compared to simulations in Ref. 11, the field should probably be smaller than assumed which can be explained by the lack of knowledge about the entrance distribution. The integrated cross sections in Fig. 5 show a similar behavior: Below 27 keV beam energy the profiles have a more homogeneous distribution with large wings. In contrast, above this energy the signal gets more peaky and at around 37 keV beam energy the best compromise is found between a Gaussian-shaped distribution and moderate wings. Above this energy, in particular demonstrated at 45 keV beam energy, the intensity within the edges already increased, a sign of overfocusing. Similar to the 2D distributions, the offset is not corrected and consequently show also a steering effect as seen in Fig. 4.

## B. Varying the applied external voltage

One unexpected result during initial tests of the detector for photodetachment beam profiles was a significant beam influence. This is summarized in Fig. 6 where in pseudocolors the beam distribution is shown at voltages from  $-2000 \dots +2000$  V jacket potential. The beam is partly collimated at the acceleration jacket because of either expelling the compensation particles of the detector area (positive potential) or attracting particles from the beam axis onto the “jacket electrodes” (negative potential; the detector acts as a drain for residual gas ions). Both effects reduce the space-charge compensation and increase the net current. It seems that the inner distribution changes and the most homogenous distributions can be found at  $-500$  V and  $+2000$  V. This happens due to the nonlinear forces caused by inhomogeneous distributions at 0 V and depends on the (net) beam

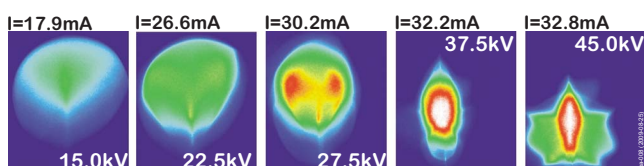


FIG. 4. (Color online) The beam distribution at different postacceleration voltages, i.e., beam energy. The current is measured with toroid 2, the transmission rises from 57% at 15 keV beam energy up to 88% at 40 keV. The color scale for each picture is the same.

current. On the other hand a bright spot appears at  $+2000$  V which is not the case for the negative equivalent. These differences with the polarity are difficult to explain with the existing data, thus experiments to refine the data are necessary. In Table I some of the data are summarized. At higher voltages of both signs the beam current variation reaches saturation. The absolute current changes are in the expected range but based on experiences with positive ion beams you would expect a higher current for positive voltages than negative. Accordingly a negative voltage should produce global decompensation: The slow compensation ions see a longitudinal potential gradient since the beam axis potential is lower near the external voltage than elsewhere which normally would mean a lower current as well. But it might be the case that the measurements of the positive potentials are falsified by attracting electrons going in the opposite direction to the  $H^-$  beam or that the possible decompensation is more than counterbalanced with fewer compensation particles (residual gas ions), i.e., lower  $H^-$  neutralization losses. The scintillator results show that secondaries probably hit the scintillator thus the signal intensities had to be corrected with the measured current of the toroid.

## C. Temporal behavior of space-charge compensation

The time-resolved behavior of the extracted current in toroids 1 and 2 is presented in Fig. 8 where a rise time is discernible of  $\approx 15 \mu s$  for the first toroid and  $\approx 40 \mu s$  for the second toroid. All signals are normalized but their maximum value is provided. The experiment has been carried out with a beam energy of 35 keV. Compared to the slow rising voltage provided by the extraction power supply the second

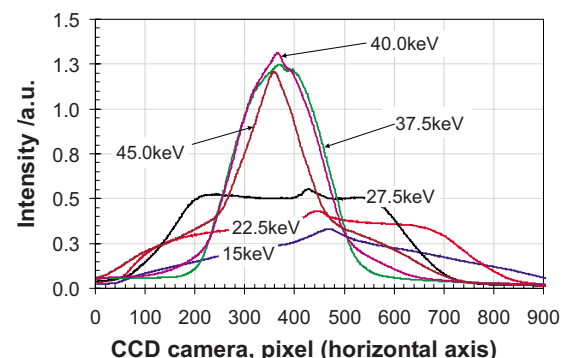


FIG. 5. (Color online) Integrated cross sections along the  $x$  axis of the beam distributions in Fig. 4. The beam energy is varied and the measured toroid currents were used to normalize the integrated signals.

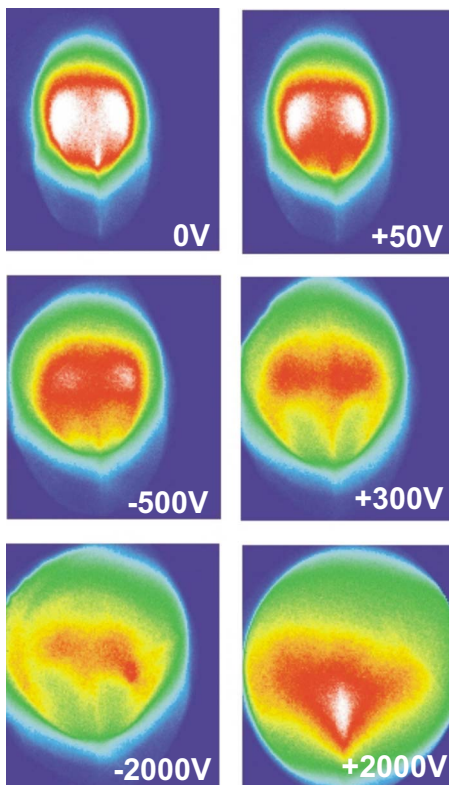


FIG. 6. (Color online) Different beam distributions for various external potentials applied to the jacket of the detector system placed in the differential pumping tank. The color scale for all pictures is the same but the intensities are corrected according the measured current in toroid 2.

toroid is closer to the 40  $\mu\text{s}$  of the extraction (this toroid has a rise time of 3–4  $\mu\text{s}$ ). You might conclude that less voltage is necessary to extract almost the whole beam current but radius and divergence angle have not stabilized, i.e., the plasma meniscus has not reached a steady state and that causes changes in the envelope which effects the transmission. Further implications concerning the extraction are a recent matter of investigation.<sup>12</sup> To use the detector as an energy analyzer the cup signal must be measured at different “jacket potentials” to provide the particle energy  $E_{\text{RGI}}$ . The pulses  $I_{\text{FDC}}(t, U_{\text{RGI}})$  are then converted to energy depending signals  $\tilde{I}(E_{\text{RGI}}, t)$  at different time steps which then has to be differentiated  $dI_{\text{RGI}}/dU_{\text{ret}}$  (see Fig. 7). The 80% clip of the

TABLE I. Some beam parameters at various voltages applied at the detector jacket; ion source current ( $36.5 \pm 0.5$ ) mA remained constant throughout the experiment. The changes refer to the current; the axis potential is calculated.

Potential $U$ (kV)	Beam current $I_2$ (mA)	Relative change (percent)	Beam axis potential (V)
-200	-32.4	+5.2	121
-100	-31.8	+3.5	119
0	-30.7 <sup>a</sup>		115
+100	-31.5	+2.5	118
+200	-30.4	-1.0	113
+300	-29.7	-3.4	112

<sup>a</sup>Beam current measured at toroid 1 is  $\approx 36$  mA and remains constant ( $\Rightarrow 17\%$  losses). This current produces a beam axis potential of 136 V and is equivalent to a perveance of 0.0045.

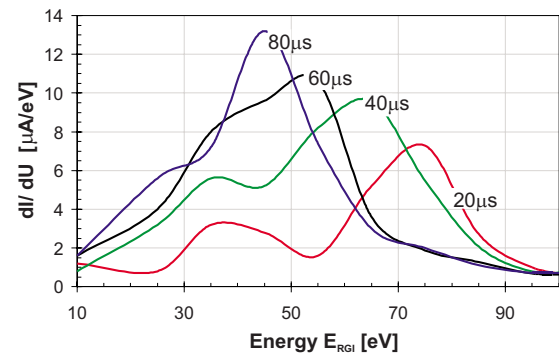


FIG. 7. (Color online) Currents of the compensation particles depending on energy and time. The energy is given by the applied voltage of the jacket potential; the magnet field is used to guide the particles into the Faraday cup. Each pulse  $I_{\text{FDC}}(t, U_{\text{RGI}})$  is then converted into  $\tilde{I}(E_{\text{RGI}}, t)$  for several time steps and eventually differentiated  $dI_{\text{RGI}}/dU_{\text{ret}}$ .

integrated value  $\int dI_{\text{RGI}}/dU_{\text{ret}} dt$  is used to define the rise time  $\tau_{\text{SCC}}$  of the space-charge compensation. But depending on plasma parameters of the ion source  $\tau_{\text{SCC}}$  is folded with the rise time of the ion beam current.

Generally, if the compensation increases the profiles get shifted to lower energies which can be seen as well in Fig. 7. The differentiated spectra seem to stop changing at about 80  $\mu\text{s}$  where also the second toroid levels off. The integrated detector current of those compensation particles compared with the beam pulses in Fig. 8 may show that at least 50% of the accumulation process is over in not more than 60  $\mu\text{s}$ , compared with the beam pulse which already reached half of the maximum in T1 and based on experience with positive ion beams where beyond 80% compensation the beam potential changes only very little. It should be mentioned that the discussion followed a “straightforward” approach which typically overestimates the duration of the space-charge compensation  $\tau_{\text{SCC}}$ . A more rigorous data analysis according to Ref. 8 may deliver a smaller rise time since a more advanced consideration of the ion source behavior.

### III. SUMMARY AND OUTLOOK

First experiments at the new FETS beam line have been carried out. The maximum current is very close to the needs of the FETS project. The measurements also suggest that the LEBT installed by end of this year is capable to deal with the beam parameters. The behavior of the postacceleration is as expected. The electrode system can improve the transporta-

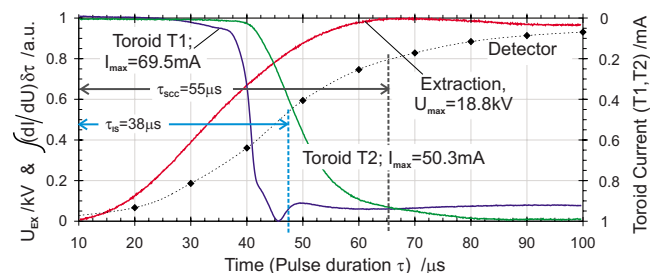


FIG. 8. (Color online) Normalized blowup of the extraction voltage, toroid 1 and 2 signals, and the energy-dependent integrated detector current of the compensation particles. The rise time of the space-charge compensation  $\tau$  is  $\approx 55$   $\mu\text{s}$ .

tion, i.e., shrinks the beam size by its lens effect. But the focal effect has to be chosen carefully to the extracted beam current and desired energy. Differences between theoretical studies and experiments can be explained by not knowing the exact starting conditions and should be complemented with empirical data. If a voltage is applied at the detector for photodetachment beam profiles the beam will be influenced considerably. An upper limit of the  $\tau_{\text{SCC}} \leq 55 \mu\text{s}$  could be estimated which includes a build up time of the ion source plasma sheath. Only preliminary studies have been performed and should be followed by more detailed measurements. That may include modifications at the detector (e.g., better shielding of the applied voltage and/or temporary changes to use the detector as a retarding energy spectrum analyzer with higher resolution).

## ACKNOWLEDGMENTS

Partners of the Front End Test Stand Collaboration are Isis Neutron Spallation Source (Rutherford Appleton Laboratory), Imperial College (London), ASTeC (Intense Beams Group), University of Warwick (UK), and University of Bilbao (Spain). The authors want to thank in particular P. Wise, M. Whitehead, T. Wood, M. Westall, D. Findlay, M. Perkins, M. Bates, and P. J. Savage for their administrative, technical, and engineering help.

- <sup>1</sup>T. R. Edgecock, Proceedings of the Sixth International Workshop Neutrino Factories and Superbeams (NuFact04), Osaka, Japan, July/August 2004.
- <sup>2</sup>A. P. Letchford, M. A. Clarke-Gayther, D. J. S. Findlay, S. R. Lawrie, P. Romano, P. Wise, S. M. H. Al Sari, S. Jolly, A. Kurup, D. A. Lee, P. Savage, J. Alonso, J. J. Back, J. Bermejo, R. Enparantza, D. C. Faircloth, J. Pasternak, J. K. Pozimski, C. Gabor, D. C. Plostinar, and J. Lucas, *Proceedings of LINAC 2008*, Victoria, British Columbia, Canada (JACoW, 2008), MOP009.
- <sup>3</sup>D. C. Faircloth, S. R. Lawrie, A. P. Letchford, C. Gabor, P. Wise, M. Whitehead, T. Wood, M. Westall, D. Findlay, M. Perkins, P. J. Savage, D. A. Lee, and J. K. Pozimski, *Rev. Sci. Instrum.* **81**, 02A721 (2010).
- <sup>4</sup>S. Jolly, D. Lee, J. Pozimski, P. Savage, D. Faircloth, and C. Gabor, *Proceedings of the DIPAC 2007*, Venice, Mestre, Italy (JACoW, 2007), WEO2A01.
- <sup>5</sup>C. Gabor, C. R. Prior, A. P. Letchford, and J. K. Pozimski, *Proceedings of the LINAC 2008*, Victoria, British Columbia, Canada (JACoW, 2008), TUP084.
- <sup>6</sup>D. A. Lee, J. K. Pozimski, C. Gabor, and P. Savage, *Proceedings of the DIPAC 2007*, Venice, Mestre, Italy (JACoW, 2007), TUPB11.
- <sup>7</sup>A. J. T. Holmes, *Phys. Rev. A* **19**, 389 (1979).
- <sup>8</sup>A. Jakob, Ph.D. thesis, Goethe-University Frankfurt, 2001.
- <sup>9</sup>D. C. Faircloth, A. P. Letchford, C. Gabor, M. O. Whitehead, T. Wood, S. Jolly, J. K. Pozimski, P. J. Savage, and M. Woods, *Rev. Sci. Instrum.* **79**, 02B717 (2008).
- <sup>10</sup>R. Keller, *The Physics and Technology of Ion Sources* (Wiley, New York, 1989), pp. 23–52.
- <sup>11</sup>D. C. Faircloth, M. Whitehead, C. Gabor, and J. K. Pozimski, *Proceedings of the EPAC08*, Magazzine del cotone, Genoa, Italy (JACoW, 2008), MOPC142.
- <sup>12</sup>S. R. Lawrie, D. C. Faircloth, A. P. Letchford, C. Gabor, and J. K. Pozimski, *Rev. Sci. Instrum.* **81**, 02A707 (2010).